Noncontact Respiration Monitoring During Sleep With Microwave Doppler Radar

Mari Zakrzewski, *Student Member, IEEE*, Antti Vehkaoja, Atte S. Joutsen, Karri T. Palovuori, and Jukka J. Vanhala, *Member, IEEE*

***Abstract*— This paper demonstrates the measurement of respiration waveform during sleep with a noncontact radar sensor. Instead of measuring only the respiration rate, the methods that allow monitoring the absolute respiration displacement were studied. Absolute respiration displacement can in theory be measured with a quadrature microwave Doppler radar sensor and using the nonlinear demodulation as the channel combining method. However, in this paper, relative respiration displacement measures were used as a reference. This is the first time that longer data sets have been analyzed successfully with the nonlinear demodulation method. This paper consists of whole-night recordings of three patients in an uncontrolled environment. The reference respiration data were obtained from a full polysomnography recorded simultaneously. The feasibility of the nonlinear demodulation in a real-life setting has been unclear. However, this paper shows that it is successful most of the time. The coverage of successfully demodulated radar data was ∼58%–78%. The use of the nonlinear demodulation is not possible in the following cases: 1) if the chest wall displacement is too small compared with the wavelength of the radar; 2) if the radar data do not form an arc-like shape in the *I Q*-plot; or 3) if there are large movement artifacts present in the data. Both in academic literature and in commercial radar devices, the data are processed based on the presumption that it forms either an arc or a line in the *I Q*-plot. Our measurements show that the presumption is not always valid.**

***Index Terms*— Doppler radar, breathing patterns, radar measurements, non-contact respiration measurement.**

I. Introduction

PEOPLE sleep roughly a third of their lifetime. Sufficiently long and good quality sleep is essential for daytime performance and well being. Chronic sleep deprivation can lead to type 2 diabetes, depression, hypertension, heart failure, stroke, memory and learning problems, as well as increased risk of traffic accidents due to daytime sleepiness [1], [2]. The largest causes of chronic sleep deprivation are sleep apnea and nocturnal movement disorders such as restless legs syndrome. In the general adult population, the prevalence of obstructive sleep apnea has been estimated to be 3–7% in men and 2–5% in women [3].

The capacity of sleep laboratories is not large enough to account for the number of sleep disorder patients. Currently, only the ones suffering from severe symptoms are diagnosed and treated. However, with early diagnosis and intervention, it is possible to increase capacity, reduce overall costs, and quickly improve patients' quality of life. Therefore, affordable and robust methods, which facilitate early detection of those in need of an intervention and/or enable low-cost follow-up of the intervention, are highly needed.

Full polysomnographic (PSG) recording is the gold standard method for sleep monitoring because it is accurate and reliable. However, there are also drawbacks in PSG recording: 1) An extensive set of measurement electrodes and other sensors need to be attached to the person. This takes approximately one hour of preparation time each night from a skilled technologist. This makes the measurement expensive and impractical to be used for monitoring longer than one or two nights. 2) Attaching several sensors to a patient may also disturb sleep, thus leading to erroneous information.

There have been numerous efforts for developing the PSG recording with a reduced or an alternative set of sensors for long-term home monitoring [4]–[6]. In clinical sleep evaluations, portable sleep monitors are mainly used in conjunction with a comprehensive sleep evaluation [7]. The recording is often called as ambulatory PSG. In current clinical practice, if certain requirements are met, an ambulatory PSG device can be used for diagnosis of obstructive sleep apnea (OSA) [6]. In that case, the portable monitor must record airflow, respiratory effort, and blood oxygenation, at minimum [7]. Examples of commercial ambulatory PSG devices include [8], [9]. Devices with only one or two sensors also exist. Commercial setups include, for example, a snore and SpO_2 sensor combination (such as WatchPAT [10]) or a single-channel device with a nasal cannula (such as ApneaLink [11], [12]). For long-term monitoring, however, these sensors unavoidably cause some inconvenience.

There are also methods that do not require the user to wear any sensors. Sleep Cycle sells a mobile application that uses nighttime microphone recording for apnea screening [13]. Force sensors placed under mattress or under the supports of the bed has been studied for detection of sleep-disordered breathing [14], [15]. Earlier works including the use of force sensors are Static charge sensitive bed (SCSB) [16] and EMFit sensor [17]. The aforementioned methods enable

Manuscript received December 31, 2014; revised June 2, 2015; accepted June 6, 2015. Date of publication June 17, 2015; date of current version August 12, 2015. This work was supported in part by TEKES–the Finnish Funding Agency for Technology and Innovation and in part by the Finnish Konkordia Fund. The associate editor coordinating the review of this paper and approving it for publication was Dr. Lorenzo Lo Monte.

M. Zakrzewski, A. S. Joutsen, K. T. Palovuori, and J. J. Vanhala are with the Department of Electronics and Communications Engineering, Tampere University of Technology, Tampere 33720, Finland (e-mail: mari.zakrzewski@tut.fi; atte.joutsen@student.tut.fi; karri.palovuori@tut.fi; jukka.vanhala@tut.fi).

A. Vehkaoja is with the Department of Automation Science and Engineering, Tampere University of Technology, Tampere 33720, Finland (e-mail: antti.vehkaoja@tut.fi).

long-term monitoring of sleep disorders and therefore facilitate also the monitoring of the effect of treatment. In more recent applications, self-monitored sleep data can be viewed with a mobile device. Beddit has developed a pressure sensor strip that is placed under the bedsheet and data analysis software for sleep data viewing [18], [19]. Wristband devices such as FitBit [20], Lark [21], and Jawbone Up [22] use a wrist-worn accelerometer to determine sleep and awake cycles. These applications are mainly targeted for consumers for long-term self-monitoring and do not measure parameters relating to apnea or other sleep disorders.

In this active field of research and development for long-term monitoring of sleep, microwave radar sensor offers one option. The first commercial products using microwave radar monitoring of sleep are bedside consumer products developed by ResMed: SleepMinder, HSL-101 for Omron, and Renew Sleep Clock for Gear4. Very recently, ResMed launched an S+ device and mobile application [23]. These devices are targeted for self-monitoring of sleep at home, and the devices can measure parameters such as sleep duration, sleep onset time, number and time of awakenings during night, and so on. In addition, S+ estimates sleep stages (light sleep, deep sleep, and REM). Moreover, Japanese Nintendo, previously known mainly for its video games, is expected to launch a sleep monitoring application that is based on Resmed technology [24].

Recently, Lee *et al.* [25] were the first to show that different types of breathing patterns can be recorded with a radar sensor. A test subject was instructed to emulate the following breathing patterns for a short time period: normal breathing, Kussmaul's breathing, Cheyne-Stokes respiration, ataxic breathing and Biot's breathing, Cheyne-Stokes variant, central sleep apnoea, and dysrhythmic breathing. The patterns were only recorded, not recognized automatically.

Quantitative analysis of radar monitoring of sleep with considerably large patient groups (n varies between 75 to 113 subjects) has been presented in [26]–[28] by ResMed. The team has gained good quantitative results with radar monitoring. The separation of sleep and wake stages with an overall per subject accuracy of 78% was presented in [27]. An automated sleep/wake pattern classification was based on measuring movements in 30 second epochs. The radar sensor was demonstrated to gain similar accuracy to wrist actigraphy for sleep/wake determination [28]. In [26], the diagnostic accuracy of SleepMinder in identifying obstructive sleep apnoea and apnoea-hypopnea index (AHI) was assessed. An accuracy of 91% was gained when a diagnostic threshold of moderate-severe (AHI $\geq$ 15 events/h) for obstructive sleep apnoea was used [26].

In this paper, we contribute to the field by presenting several qualitative analyses of radar monitoring of sleep-time respiration. A few challenges that need to be revisited in future studies are also shown. In addition, the respiration waveform measuring absolute chest wall displacement with radar sensor is shown. To be precise, the radar sensor measurement is validated against the respiration effort belt measurement that measures relative change of the ribcage circumference. The chosen reference is, however, widely used in the PSG recording. Moreover, the accurate displacement measurement with radar sensor has previously been demonstrated with simple radar targets [29], [30]. Nevertheless, the accuracy of the absolute chest wall displacement measurement still needs more validation. Chest wall displacement is proportional to the breathing depth, and for clarity, we consider the absolute chest wall displacement to correspond to the depth of the breath, while in fact, they are not quite the same thing.

The possibility of acquiring absolute chest wall displacement was recently noted in Hu *et al.* [31], and its measurement has also been reported by Massagram *et al.* [32] and by Lee *et al.* [25]. In [32], the tidal volume of eight subjects were measured during short time periods in supine and in seated positions. Lee *et al.* [25] measured the chest wall displacement in six subjects during short time periods. The measurement lengths of these studies were not reported accurately, but the presented examples suggest that it has been in the range of a few minutes. Thus, to the best of our knowledge, the presented work is the first time that longer (full night) data sets have been successfully analyzed for determination of absolute chest wall displacement.

Quadrature radar sensor produces two channels: in-phase and quadrature channels. There are two main approaches for demodulating the two channels: linear and nonlinear demodulation methods. Massagram *et al.* used the linear demodulation method (also called the principal component analysis, or PCA) to combine the two radar channels [32]. Lee *et al.*, on the other hand, used single-channel radar with 2.4 GHz transmitting frequency [25]. Thus, the null point problem will be faced, as also noted by the authors of [25]. The null point problem means that a severe signal distortion is encountered in certain radar-subject distances [33]. The problem is not necessarily seen in short time recordings, but will emerge in long-time recordings. The use of quadrature radar and the PCA method would solve the null point problem. However, the magnitude information of the displacement of the chest wall in centimeters, which describes the depth of the breath, would be lost, and only the relative respiration displacement can be measured. To the best of our knowledge, our paper is the first to report long-time breathing measurements with a quadrature radar and the nonlinear demodulation method. The use of long data sets is a notable difference compared to previous work because the long-term data inevitably contains also challenging and complex data segments.

In this paper, we study the utilization of a microwave radar sensors for sleep monitoring in a domestic environment. The study consists of whole-night recordings of three patients with a radar sensor together with a full PSG recordings. The measurements were performed outside a laboratory in a rehabilitation center without constant nurse oversight. This paper brings the large-scale commercial use of radar sensor in sleep monitoring one step further.

II. Materials and Methods

A. Microwave Radar Monitoring

Microwave Doppler radar monitoring enables ubiquitous, non-contact, through-clothes measurement of heart and respiration activity. The signal transmitted from the radar

sensor is reflected from the chest wall. The phase of the reflected signal is proportional to the small movements of the chest wall. The transmitting power of the radar is small, well below the recommendations set by Federal Communications Commission (FCC) and The European Telecommunications Standards Institute (ETSI). The quadrature radar baseband signal's in-phase(I)- and quadrature(Q)-components are expressed as:

$$\begin{aligned} B_{\mathrm{I}}(t) &= V_{\mathrm{I}} + A_{\mathrm{B}}\cos\left(\theta(t)\right) \\ &= V_{\mathrm{I}} + A_{\mathrm{B}}\cos\left(\frac{4\pi d_0}{\lambda} + \frac{4\pi x(t)}{\lambda} - \theta_0 + \Delta\phi(t)\right), \\ B_{\mathrm{Q}}(t) &= V_{\mathrm{Q}} + A_{\mathrm{B}}A_{\mathrm{E}}\sin\left(\theta(t) + \phi_{\mathrm{E}}\right) \\ &= V_{\mathrm{Q}} + A_{\mathrm{B}}A_{\mathrm{E}}\sin\left(\frac{4\pi d_0}{\lambda} + \frac{4\pi x(t)}{\lambda} - \theta_0 \right. \\ &\qquad \left. + \Delta\phi(t) + \phi_{\mathrm{E}}\right), \end{aligned} \tag{1}$$

where V_{I} and V_{Q} are DC-offset in I- and Q-channels, A_{B} is the baseband amplitude, $\theta(t)$ is the time varying displacement angle (in degrees), d_0 is the nominal distance between the radar and the subject, $x(t)$ is the time varying displacement of the chest wall (in meters), λ is the wavelength of the carrier, θ_0 is the constant phase shift, $\Delta\phi(t)$ is the residual phase noise, A_E is the amplitude imbalance, and ϕ_E is the phase imbalance.

To acquire the chest wall displacement data $x(t)$, these two channels, I and Q, need to be combined. One option for a combining method is *linear demodulation* (or PCA) [34]. PCA finds the principal component of the two-dimensional data and, in practice, approximates the arc of a circle as a line. This approximation is valid if the arc length is small enough (in other words, if the chest wall displacement is significantly smaller than the carrier wavelength, $x(t) \ll \lambda$). For respiration monitoring with a 10 GHz radar, which is used in this study, the approximation is valid with shallow respiration but is not always valid with deep respiration. Another drawback is that the PCA method loses the absolute value of the displacement information (the signal magnitude) [35]. In fact, the sign of the signal is lost as well, meaning that a displacement can not be classified as being an inspiration or an expiration. It should, however, be noted that the linear demodulation is computationally simple. Moreover, the linear demodulation can be used with small arc lengths. Therefore, if the disadvantages of the method are acceptable in the application in question, the linear demodulation may be the best choice.

Another option for channel combining is using *nonlinear demodulation*. For this, V_{I} and V_{Q} need to be estimated from a short data segment. The data forms an arc of a circle in an IQ-plot. By estimating the center of such circle, estimates of V_{I} and V_{Q} are gained [36], [37]. The selection of the best algorithm for the center estimation with radar data has been an active research topic recently. Several algorithms have been proposed such as the one presented by Park *et al.* [37], Levenberg-Marquard (LM) algorithm [36], L_1-norm-based algorithm [30], [38], gradient descent [39], [40], and least squares [30], as well as Hough transformation, particle filter, and direct phase estimation based on a difference vector [41]. The performance of the four latter algorithms has been compared in [41], but unfortunately the interpretation of the results is erroneous, because discontinuities due arctangent function are not properly removed. The Park's method is shown to suffer from a systematic error, if the respiration waveform is not single-tone sinusoidal [36]. Instead, the LM algorithm is shown to perform accurately in simulations as well as in simplified emulations with a spherical target or a planar target in two independent studies: in [36] and in [30]. The L_1-norm-based algorithm [38] might, however, be more sensitive to outliers than the LM algorithm, but more measurements are needed to prove this.

Then after the center estimation step, the nonlinear demodulation can be performed with arctangent function:

$$\hat{\theta}(t) = \arctan\left(\frac{B_{\mathrm{Q}} - \hat{V}_{\mathrm{Q}}}{B_{\mathrm{I}} - \hat{V}_{\mathrm{I}}}\right) \approx \arctan\left(\frac{A_{\mathrm{B}}\sin(\theta(t))}{A_{\mathrm{B}}\cos(\theta(t))}\right). \tag{2}$$

The arctangent function may cause discontinuities around $\frac{\pi}{2}$ or $-\frac{\pi}{2}$. These are discussed for example in [35], [40], and [42]. However, based on our experience and simulations, the use of Matlab built-in unwrap function is fully adequate for removing discontinuities.

By using nonlinear demodulation, an absolute displacement of the target can be obtained from the demodulated signal. This has previously been shown in [29] and in [30]. In [29], a half-circle radar target was moved automatically with a programmable linear stage, and the center estimation was performed with Park's method. Without any specific calibration procedures (a so-called I/Q imbalance calibration was performed, though), a small displacement of 1 cm was acquired with the accuracy of 5%. Similarly, accurate absolute displacement measures were gained with a planar radar target and the LM center estimation algorithm in [30]. In the present study, nonlinear demodulation with LM center estimation algorithm was also used.

B. Measurement Setup

The measurement setup is shown in Fig. 1. The radar was attached over the bed at the height of 1.5 m to a supporting pole. A commercial quadrature radar module, MDU4220 [43], with transmitting frequency of 10.587 GHz was used.

The beam width of the radar module used is $36^\circ \times 18^\circ$. In practice, this means that the whole torso area is in the radar coverage area. This has twofold consequences: on one hand, the areas moving most due to respiration are in the coverage area even though the patient moves slightly; on the other hand, in addition to chest movements, stomach and limb movements contribute to the backscattered signal. Moreover, the movement of the PSG unit and the movements of PSG sensor wires will contribute to the backscattered signal as well. In our study, the PSG unit was attached to the stomach strap, further away from the center of the radar beam, to decrease the echoes from the PSG unit and to allow free monitoring of the chest area movements with the radar sensor. Attachment to the chest strap would probably have caused the PSG unit to move along the cardiac activity as well.

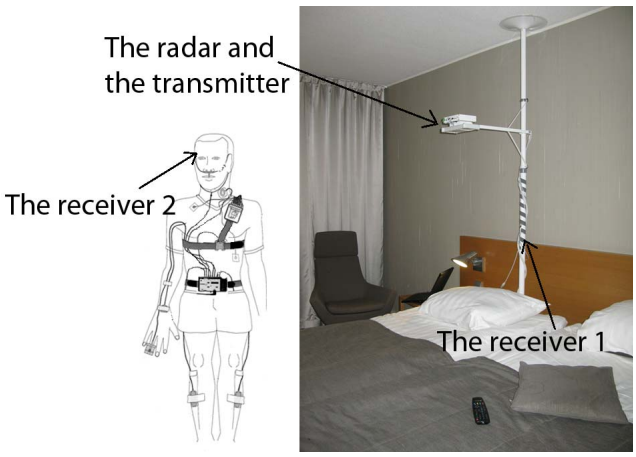

Fig. 1. The measurement setup. The radar was attached to a stand over the bed. A commercial wearable PSG device was used as a reference. The PSG recording unit was attached to the stomach strap, which allowed free monitoring of the chest area movements with the radar sensor. The synchronization receiver 1 was attached to the stand, and the receiver 2 to the forehead of the test subject.

The radar data were sampled at the sampling rate of 800 Hz with a 24-bit data acquisition (DAQ) device ADCiso4x (from Icraft). The data was collected with a laptop computer and analyzed offline.

The respiration signals obtained in a whole-night full PSG recording were used as a reference. A portable PSG device (SOMNOscreen plus, manufactured by SOMNOmedics GmbH, Germany) was used as the reference device. A portable model allowed the patient to move and walk freely in the measurement room and to go to the bathroom during the night. The used PSG setup contained a large set of sensors, including EEG, ECG, abdominal and thoracic effort, snoring (microphone), naso/oral flow, SpO_2 (oxygen saturation), position, and periodic leg movement (PLM) sensors. The PSG data were analyzed and scored by one expert scorer in Helsinki Sleep Clinic, Vitalmed, according to the American Academy of Sleep Medicine (AASM) 2007 criteria [44].

The data synchronization between the radar and the reference was assured by a synchronization system reported in detail in [45] and [46]. The radar device housed an integrated synchronization pulse transmitter. One receiver was connected to the DAQ device of the radar and one to a free channel in the PSG device.

In total, 12 test subjects were recruited and successfully recorded. However, three subjects were selected for detailed analysis for this study based on two inclusion criteria: PLM index < 10 and AHI < 10 during the recording night. The purpose of this was to show the functionality of the radar monitoring method with relatively undistorted data. PLMs, especially, cause large artifacts to the data, and automated detection and removal of them was chosen to be left as future work at this early stage of the research. The demographic data of the test subjects is shown in Table I. The Ethics Committee of Central Finland Hospital District approved the study. All subjects signed an informed consent before participating to the study.

TABLE I
DEMOGRAPHIC DATA OF THE TEST SUBJECTS AND SLEEP DATA FROM THE POLYSOMNOGRAPHY

Patient	Sex	Age	Height (cm)	Weight (kg)	AHI	PLMI	Sleep time
1	F	51	167	59	6.4	9	7 h 48 min
2	M	57	183	68	6.4	0	7 h 13 min
3	F	46	153	59	1.4	0.6	6 h 28 min

AHI = apnoea hypopnea index, PLMI = periodic leg movement index.

C. Signal Processing

1) Radar Signal Pre-Processing: Firstly, the radar data was low pass filtered with a 50 Hz anti-alias filter. All the data (both radar and PSG data) was then resampled to 100 Hz and synchronized. Secondly, the radar data was high pass filtered with a 0.1 Hz filter.

The parts of the data that contained movement artifacts were removed from the respiration analysis *manually*. This obviously is not possible in an end application and presents a limitation to this study. However, in this proof-of-concept study, we have simplified the problem by limiting only to those epochs that do not contain pronounced movement artifacts. One automated movement detection algorithm based on a threshold detection of signal power in 0.05 to 2 Hz bandwidth is presented in [27] and in [28]. This method, however, does not perform well with a 10 GHz radar as the respiration arc length is close to 50% of a whole circle, and the movement artifacts are approximately in the same order of magnitude.

In total, the percentage of discarded data was 10% for patient 1, 15% for patient 2, and 24% for patient 3. The movement artifacts may have been caused, for example, by the movements of the torso, arms, or legs as well as by coughing or sneezing. Only continuous segments longer that the epoch length ($>$120 s) were included. This partly explains the large percentages of discarded data. In addition, the parts when the subject was in an upright posture were discarded.

2) Nonlinear Demodulation: In this paper, the LM algorithm has been used as the fitting method in center estimation. The LM algorithm is an iterative least-squares fitting method, and the data mean is used as the initial guess for the algorithm. Details of the LM method are presented in [36]. The center estimation was performed in 30 s epochs.

The LM method is sensitive to large outliers. This was pointed out in [38]. After the removal of the epochs with large movement artifacts, the data still contained some smaller and fast artifacts. These outliers sometimes caused errors in the center estimates. To overcome these errors, the consecutive center estimation results were averaged. The averaging was performed by calculating the median of the four consecutive center and radius estimates. Thus, the effective epoch size in further analysis was 4×30 s = 120 s. Then, atan2-function and phase unwrapping in Matlab were used to perform the arctangent demodulation.

3) Comparison of Radar and Respiration Effort Belt Signals: The successfully demodulated radar data was then compared with the reference respiration effort belt data. The respiration effort belt measurement does not measure

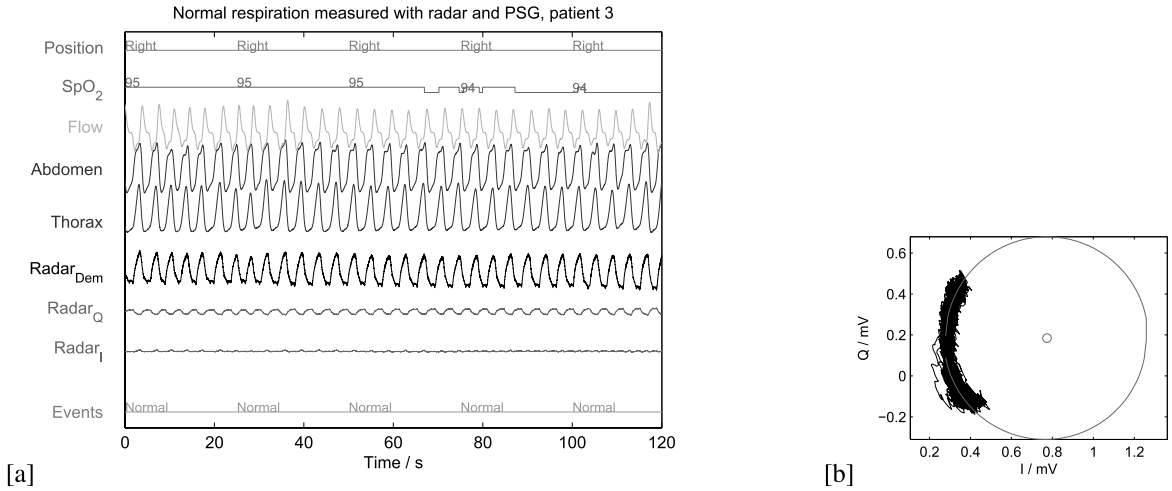

Fig. 2. An example of normal respiration successfully demodulated with the nonlinear demodulation method a) in time domain and b) in IQ-plot.

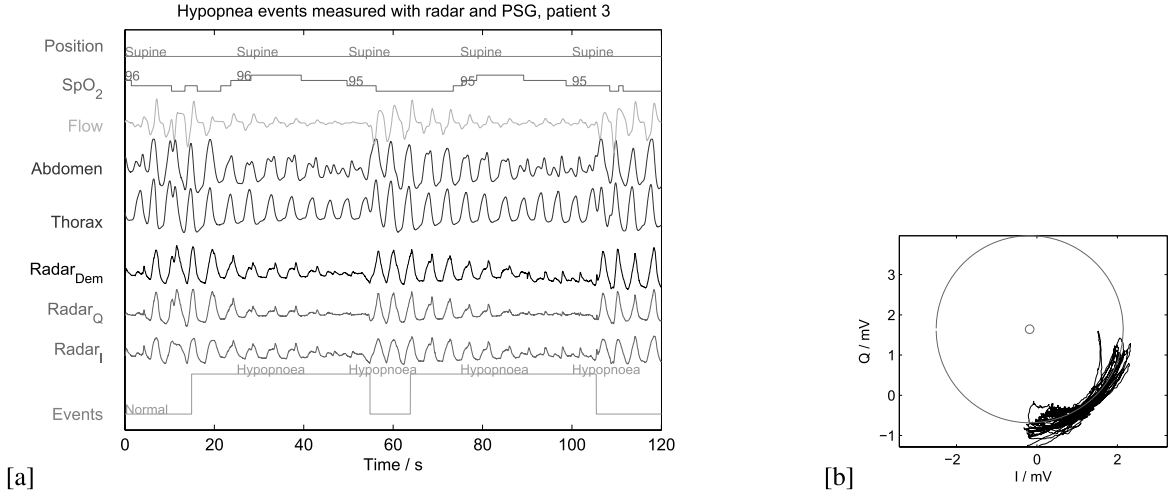

Fig. 3. An example of hypopnea events successfully demodulated with nonlinear demodulation method a) in time domain and b) in IQ-plot.

the absolute chest or abdomen wall displacement, but relative change of the ribcage circumference instead. The sensitivity of the belt sensor varies largely from posture to posture. Moreover, also the tightness of the attachment of the elastic band strongly affects the sensitivity of the sensor signal. Thus, to fairly compare the signals, the thorax and the abdomen belt signals were scaled to match the radar signals. The scaling factors were calculated epoch-wise so that the standard deviation σ of the radar and the belts' signal would be equal. The same scaling method has been used in [32].

For comparison, mean squared error (MSE) between the radar and the reference signals was calculated. MSE was calculated for the thorax and the abdomen signals separately on a per-epoch basis. To allow inter-epoch comparison, the data was first normalized to have a unit σ.

4) Comparison of Linear and Nonlinear Demodulation: The linear and the nonlinear demodulation methods were also compared. The radar data that was successfully demodulated with the nonlinear demodulation was also demodulated with the linear demodulation. Epoch-wise MSE values between the two were calculated. As the linear demodulation method loses the absolute displacement information, the data was again normalized to have a unit σ. In addition, as the linear demodulation also loses the direction of movement, the MSE values were calculated for both the resulting signal and the mirrored signal. The smaller of the two MSE values was chosen for further analysis.

III. Results

The nonlinear demodulation was successful during most epochs of the whole night measurements. Fig. 2 shows an example of a short window of data during normal breathing together with PSG respiration signals. In Fig. 3, another example of demodulated data during hypopnea events are shown. In Fig. 2, the amplitude of the data before demodulation is rather small ($\sim$0.2 mV in I-channel, $\sim$0.5 mV in Q-channel). In Fig. 3, on the other hand, the amplitude is at least fourfold ($\sim$2 mV) in both the channels. However, the measured displacement after demodulation is around 0.3 cm in both the cases. This nicely illustrates how other factors than displacement determine the amplitude of the data before demodulation.

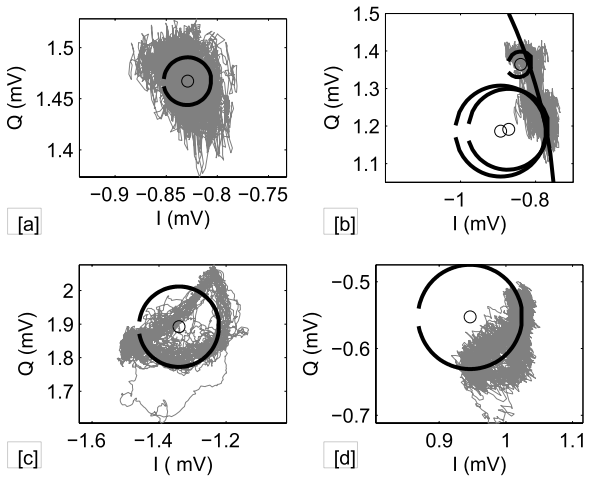

Fig. 4. In some cases, the nonlinear demodulation fails. This happens, if the arc (or the displacement) is small as in a) and b); or if the data forms a more complex shape than an arc of a circle as in c) and d). In a), the LM algorithm has returned an erroneous center estimate that is close to the mean of the data. In b), the consecutive estimates from the LM algorithm have large variation.

TABLE II
NONLINEAR DEMODULATION FAILING RATE IN EACH POSTURE

Patient		Posture				All postures
		Supine	Right	Left	Prone	
1	F [%]	55	26	43	–	42
	t [hh:mm]	02:07	01:57	03:46	–	07:50
2	F [%]	60	24	29	–	34
	t [hh:mm]	01:33	02:35	03:06	–	07:14
3	F [%]	55	25	16	16	22
	t [hh:mm]	00:35	01:05	03:19	00:33	05:33

F = the proportion of failed segments in each posture, t = the time a patient spend in the respective posture without moving during the measurement night.

However, the nonlinear demodulation fails in the following two cases:

1) The resulting arc length is too small to contain sufficient information of the circle curvature. In this case, the resulting circle estimates are arbitrary: either the circle is estimated close to mean of the data (see Fig. 4a), or the estimated circle is overly large and the center estimates of the consecutive data windows have large variation (see Fig. 4b). Note that Fig. 4b shows circle estimates from four consecutive data windows. The fourth circle estimate is so large that only a small arc is seen in the plot. In the first case, the center estimation algorithm converges to the initial guess (the data mean was used as the initial guess), and in the latter, the center estimation sometimes converges towards infinity.
2) In some cases, the data does not form an arc in the IQ-plot but a more complex shape instead. This is shown in Fig. 4c and 4d.

The data segments were examined *manually* to separate successful and failed segments. The number and length of these failed segments vary significantly between the subjects and sleeping postures. The proportion of failed segments in each posture are shown in Table II. Note that, data discarded

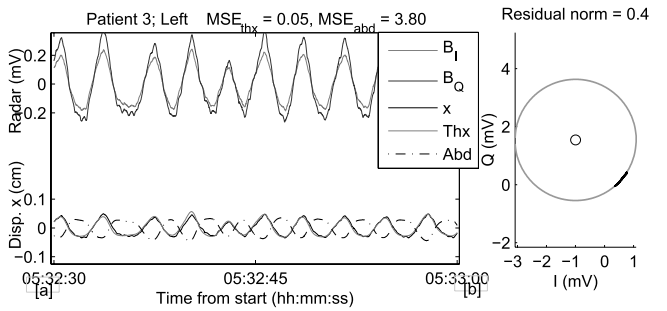

Fig. 5. An example of a large amplitude in the I- and the Q-channel data, B_{I} and B_{Q}, but with a small displacement x after demodulation. The data are shown a) in time domain and b) in IQ-plot. Thx = thorax and Abd = abdomen.

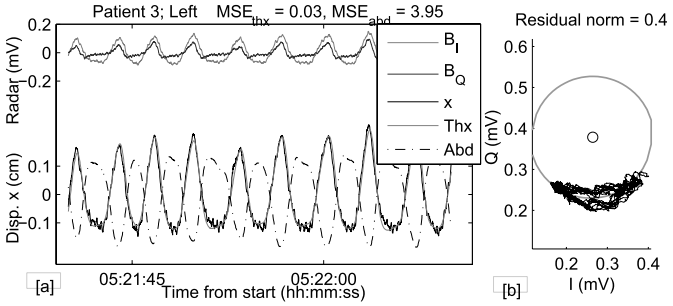

Fig. 6. An example of a small amplitude in the I- and the Q-channel data (B_{I} and B_{Q}), but with a large displacement x after demodulation. The data are shown a) in time domain and b) in IQ-plot.

due to movements were not included in these values. It seems, that the failing rate was lower, when a patient was in right, left, or prone postures. Both types of failed segments were seen in all the postures. However, the case 1 fails were dominant when the patient was lying on the left side, and the case 2 fails were dominant when the patient was supine.

Examples of successfully demodulated radar data compared with the respiration belt signals are shown in Figs. 5–9. The examples are selected to represent multiple different effects seen in the data. The top left curves (in Fig. 5a) are I- and Q channels, B_{I} and B_{Q}, before demodulation. The bottom left curves in the same figure are the demodulated signal and the reference thorax and the abdomen belt signals. In the right-hand side (in Fig. 5b), B_{I} and B_{Q} are plotted in IQ-plot together with the estimated circle. The residual error of the center estimation is shown in the top. This same order is used in the following figures as well.

Figs. 5 and 6 present successful demodulation with short and large arc length cases. Fig. 5 shows a relatively large amplitude ($\sim$0.5 mV) in B_{I} and in B_{Q}, but a relatively small arc length in IQ-plot, and thus, relatively small displacement ($\sim$1 mm). An opposite case is seen in Fig. 6 with a small amplitude in B_{I} and in B_{Q} ($\sim$0.15 mV) and a large amplitude in displacement ($\sim$3.8 mm). This illustrates in practice how a small amplitude in I- and Q-channels tells nothing about the displacement. Figs. 5 and 6 also present the difference in data deviation from an arc in the IQ-plot.

Fig. 7 illustrates an example of data with varying displacement amplitudes demodulated successfully.

TABLE III

RADAR VERSUS THE BELT MEASUREMENT; THE MEAN OF EPOCH-WISE MSE VALUES FOR DIFFERENT POSITIONS; NORMALIZED DATA

		Accurate acquisition				Aligned			
Patient	Belt	Supine	Right	Left	Prone	Supine	Right	Left	Prone
1	thorax	0.71	0.34	0.30	–	0.28	0.23	0.14	–
	abdomen	0.45	0.20	0.71	–	0.22	0.17	0.44	–
	min	0.45	0.17	0.20	–	0.21	0.12	0.12	–
2	thorax	0.42	0.20	0.38	–	0.17	0.13	0.18	–
	abdomen	0.41	0.18	0.26	–	0.24	0.13	0.18	–
	min	0.33	0.15	0.24	–	0.14	0.10	0.10	–
3	thorax	0.29	0.22	0.32	0.28	0.11	0.08	0.09	0.16
	abdomen	0.24	0.57	1.03	0.22	0.19	0.18	0.14	0.18
	min	0.19	0.20	0.26	0.19	0.10	0.07	0.08	0.14

On the left, the radar and the reference data had synchronous acquisition. On the right, the data were aligned based on the maximum covariance. Patients 1 and 2 did not sleep in a prone position.

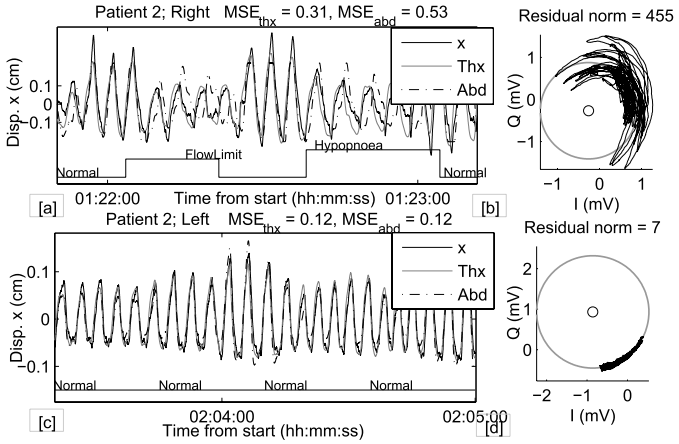

Fig. 7. An example of a successful demodulation of data containing varying displacement amplitudes. a) b) During normal breathing segments, the thorax and abdomen move synchronously, whereas during hypopnea events, a phase difference is seen in respiration belts. This results in a large MSE. c) d) Amplitude changes are seen also during normal breathing. In this case, all the signals have the same phase, and thus, the MSE is small. In the right, the data are shown in time domain, and in the left, the same data are in IQ-plot.

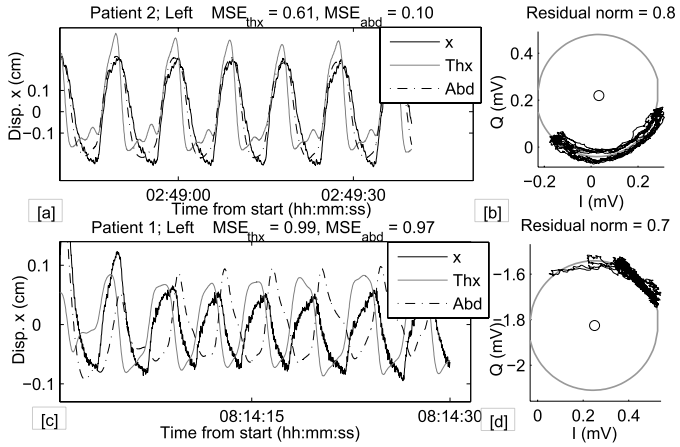

Fig. 8. An example of the thorax and abdomen moving in different phases. a) b) The radar signal follows the abdomen belt signal in this case. c) d) The respiration belts are in the opposite phases. Also, the radar signal has a different phase, thus, resulting in a large MSE. In the right, the data are shown in time domain, and in the left, the same data are in IQ-plot.

Amplitude changes can occur in data both during hypopnea events (Fig. 7a) or during a normal breathing pattern (Fig. 7b).

The relative MSE values calculated between the demodulated and normalized radar respiration signals and normalized the thorax and abdomen belt signals are shown in the left side of Table III for each patient in different positions separately. The shown values are the mean of the epoch-wise MSE values for the whole night.

The calculated MSE values are occasionally large. There are two effects that cause the large MSE values. Firstly, the thorax and abdomen do not always move synchronously. This is illustrated in Fig. 8. In Fig. 8a, the radar signal follows the abdomen signal well, whereas the thorax has a different movement pattern. In similar cases, the radar signal often follows either of the respiration belt signals. Therefore in Table III, the mean of the minimum of the two epoch-wise MSE values are also shown. However, it is not uncommon that the radar signal has a different phase to both the belt signals, as in Fig. 8b. In this case, the patient is lying on her left side,

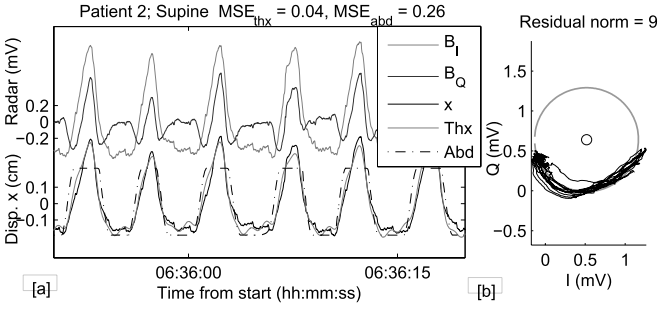

Fig. 9. In this example, the abdomen belt's signal is clipped, thus, increasing MSE. This is also a nice example of the null point problem discussed in the introduction. B_Q is in the null point, which appears as two peaks in one respiration cycle. Data are shown a) in time domain and b) in IQ-plot.

while the radar is measuring the movements of the right side. Secondly, the respiration belts do not measure the absolute displacement values. On the contrary, a patient movement results in a change in the sensitivity of the belt sensor signal. Occasionally, a belt's signal is also clipped. This is seen in Fig. 9 with the abdomen belt. Obviously, a large MSE value

TABLE IV
NONLINEAR VERSUS LINEAR DEMODULATION; THE MEAN OF EPOCH-WISE MSE VALUES FOR DIFFERENT POSITIONS; NORMALIZED DATA

Patient	Supine	Right	Left	Prone
1	0.016	0.004	0.020	–
2	0.014	0.007	0.008	–
3	0.043	0.004	0.007	0.003

is resulted. These drawbacks with the used respiration belts are, however, well known [47]. Therefore, a large MSE value does not necessarily mean bad radar data, but rather shows the limitations of the chosen reference method.

To decrease some effects caused by the asynchronous movement of the thorax and the abdomen, the second set of MSE values were calculated. For this, the respiration belt data were shifted in the time domain with the amount that maximized the crosscovariance between the radar data. The resulting MSE values are shown in the right side of Table III. It is clear that this alignment considerably decreases the MSE.

The MSE between the linear and the nonlinear demodulation methods are shown in Table IV. The difference between the demodulation methods is quite small in the data set included in the calculation.

IV. DISCUSSION

The two cases when the nonlinear demodulation fails are different in nature and should be treated differently. In case 1, the nonlinear demodulation fails, but linear demodulation can be experimented instead. With linear demodulation, however, the absolute chest wall displacement information is lost.

In case 2, however, the linear demodulation will also fail. As a matter of fact, a good method to deal with the demodulation in this kind of case has not been proposed. Likely, a source separation step, using for example a blind source separation method as the one used in [48] should be performed before the demodulation.

Aardal *et al.* [49] suggested that, at least in some cases, the center of the respiratory and cardiac activity would not be the same. This is also sensible, as a smaller portion of the chest is moving due to the cardiac activity than due to the respiratory activity. Aardal *et al.* suggested that the single reflector model should be abandoned and a multiple reflector model should be used instead. The same conclusion is also drawn by Li *et al.* in [50]. Their simulations with a so-called Ray-tracing model showed that when the signal is reflected from two distinct points of the body, there are deformation effects in the resulting data in the IQ-plot. This is caused by a different phase offset in the data reflected by the two points. Salmi *et al.* [51] performed simulations and short-time real data measurements to study the single and the multiple reflection models for heart and respiration rate estimation. They concluded that nonlinear demodulation performs very well, if the radar is close to chest of a person and proposing it to be a single reflector case. However at larger distances, the method fails due to multiple reflections.

Therefore based on these previous work and this study, it seems that the single reflector model is not always adequate for sleep monitoring applications. An important question for future work is, how to deal with this.

Case 2 (not shaped like an arc) is also highly interesting, since this type of a problem has not been reported by the ResMed-team [23], [26]–[28] or by Lee *et al.* [25]. Now, there is no reason to expect that a similar, although possibly smaller, effect would not happen with the sensors used by other research groups. Nevertheless, the effect remains hidden when using the linear demodulation, as has been used by ResMed, or single-channel radar, as has been used by Lee *et al.* In such cases, there will just be unexplainable distortion in the resulting demodulated signal.

The MSE values calculated in this study are admittedly larger than the ones presented in [25]. However, the comparison is not straightforward. In [25], the MSE values are calculated from a few minutes of data from a controlled measurement. This paper presents results from whole-night measurements in an uncontrolled environment. In addition, it is not explained in [25] whether the radar and the reference data are aligned based on the data waveform itself or based on synchronous acquisition. Due to the synchronization system used in this study, the data synchronization is assured very accurately. However in different sides of the torso, the respiration movement can have different phase shifts. Thus, when comparing the data measured with a radar and with belts, the comparison is more reasonable between the aligned data than between the synchronous data. Moreover, this study contained measurements from different patient postures (supine, right, left, prone), whereas [25] and [32] contained measurements only from in front of a patient.

When comparing the performance of linear and nonlinear demodulation, the overall performance of the methods seems relatively similar. However, the difference appears with long arc lengths meaning in deep respiration. In addition, the result strongly depends on the chosen radar transmitting frequency. The linear demodulation has the advantage of being computationally simpler than the nonlinear demodulation, whereas the nonlinear demodulation can provide absolute displacement measures and the separation between the inspiration and the expiration. Thus, if a relative displacement measure is adequate for the application, the linear demodulation may be a more favorable choice.

Multiple questions remain for future work. The length of the epochs used for center estimation in this study was probably not optimal. The length of the epochs should be long enough to contain enough respiration for accurate estimation, but short enough not to contain movement artifacts from the torso or limbs. Particularly, the epoch should be longer than a typical apnea event, since during an apnea event, the signal probably does not contain enough arc length for the center estimation. Therefore, an approach that uses multiple epoch lengths simultaneously might provide a good solution. Moreover, there will be a signal discontinuity point and a sensitivity change in the point where two consecutive epochs result in different center estimates. This problem has not been addressed in the literature. It should be pointed out, that

these discontinuities are different from the ones caused by arctangent function. In addition, the automatic selection of linear or nonlinear demodulation based on data would increase the coverage of correctly processed data.

V. Conclusion

In this paper, we have successfully demonstrated the measurement of respiration waveform with a non-contact radar sensor from three full-night recordings. The results were achieved by using quadrature microwave radar sensor and the nonlinear demodulation method. The nonlinear demodulation means using a center estimation method and the arctangent channel combining method. However, the use of the nonlinear demodulation method is not possible in certain cases:

1) If the arc length of the respiration is too small, the variance of center estimates is large, and the result of the center estimation algorithm becomes arbitrary. In these cases, the linear demodulation method may work better for channel combining, however, with the result of losing the absolute displacement information.
2) If the quadrature data does not form the arc of a circle in the IQ-plot, but a more complex shape. This is most likely due to a different phase offset from multiple reflection points. In this case, an intelligent source separation algorithm could solve the problem.
3) During the sections of large motion artifacts.

Absolute target displacement measurements have previously been demonstrated with the nonlinear demodulation method. This study is the first time that the nonlinear demodulation method with a radar sensor has been demonstrated using long data sets and a real-life setting outside a controlled laboratory.

This paper serves as preliminary work, building a foundation for the use of microwave radar as a non-contact monitor of breathing patterns. It suggests that the radar method can be used as an alternative to traditional respiration monitors to provide a more convenient measurement. Naturally, extensive clinical trials are needed before proceeding with commercial or clinical use of the proposed methods.

Acknowledgment

The authors would like to thank colleagues at the University of Jyväskylä, Department on Health Sciences, for patient recruiting and for their help in collecting the reference data.

References

[1] T. Young, P. E. Peppard, and D. J. Gottlieb, "Epidemiology of obstructive sleep apnea: A population health perspective," *Amer. J. Respirat. Critical Care Med.*, vol. 165, no. 9, pp. 1217–1239, 2002.

[2] P.-O. Haraldsson, C. Carenfelt, and C. Tingvall, "Sleep apnea syndrome symptoms and automobile driving in a general population," *J. Clin. Epidemiol.*, vol. 45, no. 8, pp. 821–825, 1992. [Online]. Available: http://www.sciencedirect.com/science/article/pii/089543569290064T

[3] A. Lurie, "Obstructive sleep apnea in adults: Epidemiology, clinical presentation, and treatment options," *Adv. Cardiol.*, vol. 46, pp. 1–42, Oct. 2011.

[4] W. W. Flemons *et al.*, "Home diagnosis of sleep apnea: A systematic review of the literature: An evidence review cosponsored by the American Academy of Sleep Medicine, the American College of Chest Physicians, and the American Thoracic Society," *Chest*, vol. 124, no. 4, pp. 1543–1579, Oct. 2003. [Online]. Available: http://dx.doi.org/10.1378/chest.124.4.1543

[5] M. D. Ghegan, P. C. Angelos, A. C. Stonebraker, and M. B. Gillespie, "Laboratory versus portable sleep studies: A meta-analysis," *Laryngoscope*, vol. 116, no. 6, pp. 859–864, 2006. [Online]. Available: http://dx.doi.org/10.1097/01.mlg.0000214866.32050.2e

[6] N. A. Collop *et al.*, "Obstructive sleep apnea devices for out-of-center (OOC) testing: Technology evaluation," *J. Clin. Sleep Med.*, vol. 7, no. 5, pp. 531–548, 2011.

[7] N. A. Collop *et al.*, "Clinical guidelines for the use of unattended portable monitors in the diagnosis of obstructive sleep apnea in adult patients. Portable monitoring task force of the American Academy of Sleep Medicine," *J. Clin. Sleep Med.*, vol. 3, no. 7, pp. 737–747, 2007.

[8] D. J. Lesser, G. G. Haddad, R. A. Bush, and M. S. Pian, "The utility of a portable recording device for screening of obstructive sleep apnea in obese adolescents," *J. Clin. Sleep Med.*, vol. 8, no. 3, pp. 271–277, 2012.

[9] R. Santos-Silva *et al.*, "Validation of a portable monitoring system for the diagnosis of obstructive sleep apnea syndrome," *Sleep*, vol. 32, no. 5, pp. 629–636, 2009.

[10] E. Körkuyu *et al.*, "The efficacy of Watch PAT in obstructive sleep apnea syndrome diagnosis," *Eur. Arch. Oto-Rhino-Laryngol.*, vol. 272, no. 1, pp. 111–116, 2015. [Online]. Available: http://dx.doi.org/10.1007/s00405-014-3097-0

[11] H. Chen, A. A. Lowe, Y. Bai, P. Hamilton, J. A. Fleetham, and F. R. Almeida, "Evaluation of a portable recording device (*ApneaLink*) for case selection of obstructive sleep apnea," *Sleep Breathing*, vol. 13, no. 3, pp. 213–219, 2009. [Online]. Available: http://dx.doi.org/10.1007/s11325-008-0232-4

[12] M. K. Erman, D. Stewart, D. Einhorn, N. Gordon, and E. Casal, "Validation of the ApneaLink for the screening of sleep apnea: A novel and simple single-channel recording device," *J. Clin. Sleep Med.*, vol. 3, no. 4, pp. 387–392, 2007.

[13] *Sleep Cycle*. [Online]. Available: http://www.sleepcycle.com/, accessed Dec. 30, 2014.

[14] G. Guerrero *et al.*, "Detection of sleep-disordered breating with pressure bed sensor," in *Proc. 35th Annu. Int. Conf. IEEE Eng. Med. Biol. Soc. (EMBC)*, Jul. 2013, pp. 1342–1345.

[15] Z. T. Beattie, T. L. Hayes, C. Guilleminault, and C. C. Hagen, "Accurate scoring of the apnea–hypopnea index using a simple non-contact breathing sensor," *J. Sleep Res.*, vol. 22, no. 3, pp. 356–362, 2013. [Online]. Available: http://dx.doi.org/10.1111/jsr.12023

[16] O. Polo, L. Brissaud, B. Sales, A. Besset, and M. Billiard, "The validity of the static charge sensitive bed in detecting obstructive sleep apnoeas," *Eur. Respirat. J.*, vol. 1, no. 4, pp. 330–336, 1988.

[17] J. Alametsä *et al.*, "Automatic detection of spiking events in EMFi sheet during sleep," *Med. Eng. Phys.*, vol. 28, no. 3, pp. 267–275, 2006. [Online]. Available: http://www.sciencedirect.com/science/article/pii/S1350453305001438

[18] J. Paalasmaa, M. Waris, H. Toivonen, L. Leppäkorpi, and M. Partinen, "Unobtrusive online monitoring of sleep at home," in *Proc. Annu. Int. Conf. IEEE Eng. Med. Biol. Soc. (EMBC)*, Aug./Sep. 2012, pp. 3784–3788.

[19] Beddit. [Online]. Available: http://www.beddit.com/, accessed Jul. 30, 2014.

[20] Fitbit. [Online]. Available: http://www.fitbit.com, accessed Dec. 1, 2014.

[21] Lark. [Online]. Available: http://www.lark.com, accessed Dec. 1, 2014.

[22] Jawbone. [Online]. Available: http://www.jawbone.com, accessed Dec. 1, 2014.

[23] ResMed. [Online]. Available: https://sleep.mysplus.com/, accessed Dec. 26, 2014.

[24] Nintendo. [Online]. Available: http://www.nintendo.co.jp/ir/en/library/events/141030/05.html, accessed Nov. 8, 2014.

[25] Y. S. Lee, P. N. Pathirana, C. L. Steinfort, and T. Caelli, "Monitoring and analysis of respiratory patterns using microwave Doppler radar," *IEEE J. Transl. Eng. Health Med.*, vol. 2, no. 1800912, Oct. 2014.

[26] A. Zaffaroni *et al.*, "Assessment of sleep-disordered breathing using a non-contact bio-motion sensor," *J. Sleep Res.*, vol. 22, no. 2, pp. 231–236, 2013.

[27] P. de Chazal *et al.*, "Sleep/wake measurement using a non-contact biomotion sensor," *J. Sleep Res.*, vol. 20, no. 2, pp. 356–366, 2011. [Online]. Available: http://dx.doi.org/10.1111/j.1365-2869.2010.00876.x

[28] M. Pallin *et al.*, "Comparison of a novel non-contact biomotion sensor with wrist actigraphy in estimating sleep quality in patients with obstructive sleep apnoea," *J. Sleep Res.*, vol. 23, no. 4, pp. 475–484, 2014.

[29] X. Gao, A. Singh, E. Yavari, V. Lubecke, and O. Boric-Lubecke, "Non-contact displacement estimation using Doppler radar," in *Proc. Annu. Int. Conf. IEEE Eng. Med. Biol. Soc. (EMBC)*, Aug./Sep. 2012, pp. 1602–1605.

[30] S. Guan, J. A. Rice, C. Li, and C. Gu, "Automated DC offset calibration strategy for structural health monitoring based on portable CW radar sensor," *IEEE Trans. Instrum. Meas.*, vol. 63, no. 12, pp. 3111–3118, Dec. 2014.

[31] W. Hu, Z. Zhao, Y. Wang, H. Zhang, and F. Lin, "Noncontact accurate measurement of cardiopulmonary activity using a compact quadrature Doppler radar sensor," *IEEE Trans. Biomed. Eng.*, vol. 61, no. 3, pp. 725–735, Mar. 2014.

[32] W. Massagram, N. Hafner, V. Lubecke, and O. Boric-Lubecke, "Tidal volume measurement through non-contact Doppler radar with DC reconstruction," *IEEE Sensors J.*, vol. 13, no. 9, pp. 3397–3404, Sep. 2013.

[33] A. D. Droitcour, O. Boric-Lubecke, V. M. Lubecke, J. Lin, and G. T. A. Kovacs, "Range correlation and I/Q performance benefits in single-chip silicon Doppler radars for noncontact cardiopulmonary monitoring," *IEEE Trans. Microw. Theory Techn.*, vol. 52, no. 3, pp. 838–848, Mar. 2004.

[34] A. D. Droitcour, "Non-contact measurement of heart and respiration rates with a single-chip microwave Doppler radar," Ph.D. dissertation, Dept. Elect. Eng., Stanford Univ., Stanford, CA, USA, 2006.

[35] J. Wang, X. Wang, L. Chen, J. Huangfu, C. Li, and L. Ran, "Noncontact distance and amplitude-independent vibration measurement based on an extended DACM algorithm," *IEEE Trans. Instrum. Meas.*, vol. 63, no. 1, pp. 145–153, Jan. 2014.

[36] M. Zakrzewski, H. Raittinen, and J. Vanhala, "Comparison of center estimation algorithms for heart and respiration monitoring with microwave Doppler radar," *IEEE Sensors J.*, vol. 12, no. 3, pp. 627–634, Mar. 2012.

[37] B.-K. Park, O. Boric-Lubecke, and V. M. Lubecke, "Arctangent demodulation with DC offset compensation in quadrature Doppler radar receiver systems," *IEEE Trans. Microw. Theory Techn.*, vol. 55, no. 5, pp. 1073–1079, May 2007.

[38] W. Xu, C. Gu, C. Li, and M. Sarrafzadeh, "Robust Doppler radar demodulation via compressed sensing," *Electron. Lett.*, vol. 48, no. 22, pp. 1428–1430, Oct. 2012.

[39] Q. Lv *et al.*, "High dynamic-range motion imaging based on linearized Doppler radar sensor," *IEEE Trans. Microw. Theory Techn.*, vol. 62, no. 9, pp. 1837–1846, Sep. 2014.

[40] Q. Lv, T. Hu, S. Qiao, Y. Sun, J. Huangfu, and L. Ran, "Non-contact detection of Doppler bio-signals based on gradient decent and extended DACM algorithms," in *Proc. IEEE MTT-S Int. Microw. Workshop Ser. RF, Wireless Technol. Biomed. Healthcare Appl. (IMWS-BIO)*, Dec. 2013, pp. 1–3.

[41] H. Noguchi, H. Kubo, T. Mori, T. Sato, and H. Sanada, "Signal phase estimation for measurement of respiration waveform using a microwave Doppler sensor," in *Proc. 35th Annu. Int. Conf. IEEE Eng. Med. Biol. Soc. (EMBC)*, Jul. 2013, pp. 6740–6743.

[42] J. Wang, X. Wang, Z. Zhu, J. Huangfu, C. Li, and L. Ran, "1-D microwave imaging of human cardiac motion: An *ab-initio* investigation," *IEEE Trans. Microw. Theory Techn.*, vol. 61, no. 5, pp. 2101–2107, May 2013.

[43] Microwave Solutions Limited. *MDU4220 Datasheet*. [Online]. Available: http://www.microwave-solutions.com/shop/modules/mdu4220.html, accessed Jun. 1, 2014.

[44] C. Iber, S. Ancoli-Israel, A. J. Chesson, and S. Quan, *The AASM Manual for the Scoring of Sleep and Associated Events: Rules, Terminology and Technical Specifications*, 1st ed. Westchester, IL, USA: American Academy of Sleep Medicine, 2007.

[45] M. Zakrzewski, A. Joutsen, J. Hännikäinen, and K. Palovuori, "A versatile synchronization system for biomedical sensor development," in *Proc. 13th Mediterranean Conf. Med. Biol. Eng. Comput.*, Sevilla, Spain, Sep. 2013, pp. 951–954.

[46] M. Zakrzewski. *Synchronization System*. [Online]. Available: https://wiki.tut.fi/SmartHome/SynchronizationSystem/WebHome, accessed Dec. 1, 2014.

[47] R. B. Berry *et al.*, "Rules for scoring respiratory events in sleep: Update of the 2007 AASM manual for the scoring of sleep and associated events. Deliberations of the sleep apnea definitions task force of the American Academy of Sleep Medicine," *J. Clin. Sleep Med.*, vol. 8, no. 5, pp. 597–619, 2012.

[48] M. Zakrzewski and J. Vanhala, "Separating respiration artifact in microwave Doppler radar heart monitoring by independent component analysis," in *Proc. IEEE Sensors*, Nov. 2010, pp. 1368–1371.

[49] Ø. Aardal, S.-E. Hamran, T. Berger, Y. Paichard, and T. S. Lande, "Chest movement estimation from radar modulation caused by heartbeats," in *Proc. IEEE Biomed. Circuits Syst. Conf. (BioCAS)*, Nov. 2011, pp. 452–455.

[50] C. Li and J. Lin, "Random body movement cancellation in Doppler radar vital sign detection," *IEEE Trans. Microw. Theory Techn.*, vol. 56, no. 12, pp. 3143–3152, Dec. 2008.

[51] J. Salmi, O. Luukkonen, and V. Koivunen, "Continuous wave radar based vital sign estimation: Modeling and experiments," in *Proc. IEEE Radar Conf.*, May 2012, pp. 0564–0569.

Mari Zakrzewski (S'15) received the M.Sc. (Hons.) degree in electrical engineering from the Tampere University of Technology (TUT), Tampere, Finland, in 2005, where she is currently pursuing the Ph.D. degree.

She has been a Researcher with the Department of Electronics, TUT, since 2005. Her research interests include microwave radar monitoring of physiological signals, unobtrusive measurement technologies, smart home applications, film-type piezoelectric touch panels, and LED integration into textiles.

Antti Vehkaoja received the M.Sc. degree in electrical engineering and the D.Sc. degree in automation science from the Tampere University of Technology (TUT), Tampere, Finland, in 2004 and 2015, respectively.

He is currently a Post-Doctoral Researcher with the Sensor Technology and Biomeasurements Research Group, Department of Automation Science and Engineering, TUT. His research interests include unobtrusive physiological monitoring systems, systems for continuous health monitoring, and processing of physiological signals.

Atte S. Joutsen received the M.Sc. and L.Sc. degrees in biomedical engineering from the Tampere University of Technology (TUT), Tampere, Finland, in 2002 and 2014, respectively, where he is currently pursuing the Ph.D. degree in biomedical engineering. He received Medical Physicist qualifications from Oulu University, Oulu, Finland, in 2014. He is currently with Clothing Plus, Kankaanpää, Finland. From 2003 to 2014, he was a Medical Physicist with Tampere University Hospital, Southern Ostrobothnia Central Hospital, and the Central Hospital of Central Finland. From 2007 to 2014, he was a Researcher with TUT. Since 2008, he has been a Consultant in medical imaging radiation protection. His research interests include biopotential electrode technologies, measurements (in particular, EEG and ECG), and their signal processing in medical and consumer applications. He received the Best Presentation Award from the iBiomep Graduate School Seminar in 2011.

Karri T. Palovuori received the M.S. degree in computer engineering and the Ph.D. degree in electronics from the Tampere University of Technology (TUT), Finland, in 1991 and 1998, respectively.

He has been a Full Professor with the Department of Electronics, TUT, since 2000. His research interests include virtual environment implementation technologies, immaterial displays, and energetic systems. He has been developing new interaction methods for fogscreen displays, measurement methods for propellants and explosives, and acoustic bullet trajectory detection. He has served as a Consulting Counter-Terrorist Advisor for the national authorities since 1997. He holds ten patents.

Prof. Palovuori's awards include the Presidential InnoSuomi Award in 2003.

Jukka J. Vanhala (M'97) received the M.Sc. degree in electrical engineering, the Lic.Tech. degree in software systems and microelectronics, and the Dr.Tech. degree from the Tampere University of Technology (TUT), Tampere, Finland, in 1984, 1990, and 1998, respectively.

He was a Researcher with the Departments of Software Engineering and Microelectronics, TUT, from 1983 to 1994. From 1990 to 1991, he was a Post-Doctoral Researcher with IBM Kingston, Scientific Engineering Computations Department, NY, USA. From 1994 to 1997, he was with the Special Systems Division, Instrumentation Ltd. Since 1997, he has been a Professor with the Department of Electronics and Telecommunications Engineering, TUT. Since 2005, he has been an Adjunct Professor of Interactive Technology with the Department of Computer Sciences, University of Tampere. He has authored over 100 articles. His research interests include embedded systems, ambient intelligence, intelligent textiles, and wearable systems.

Mr. Vanhala has been a member and the Chairman of the Electronics Chapter of the Finnish Scientific Advisory Board for Defense since 2008.